Linearized Y-coupler Modulator Based on Domain-inverted Polymeric Waveguide

Dechang An, Suning Tang*, ZuZhou Yue, John Taboada,
Lin Sun, Zhong Han, Xuejun Lu, and Ray T. Chen

Microelectronics Research Center,
University of Texas at Austin, Austin, TX 78758
*Radiant Research, Inc., Austin, TX 78758

Abstract

Electro-optic polymer-based modulators have been investigated intensively due to their potential applications in optical communication systems. In this paper, we report a polymeric modulator with a domain-inverted Y-coupler configuration. Both of the modulation depth and linearity were improved due to the novel device structure. The Y-coupler modulator was automatically set at 3dB point with no need of DC bias, which eliminate the DC drift phenomena in Mach-Zehnder or co-directional modulators. At the same time, a domain-inversion poling technique was developed, which can be used to fabricate other type of active EO devices in the future.

Keywords: Y-coupler, electro-optic polymer, electro-optic modulator, polymeric modulator, modulation linearity, domain-inverted waveguide.

Electro-optic (EO) modulators, based on both inorganic crystals and polymer materials, have been investigated widely due to their potential applications in broadband communications [1-12]. Among these modulators, Mach-Zehnder interferometer and co-directional coupler are two typical structures, where a DC bias is usually needed to operate the modulators about their half-power points. The optical modulation depth is chosen to be as large as possible without introducing unacceptable distortion. However, it is difficult to set these kinds of modulators precisely to the 3dB points due to the DC drift phenomena [13-15].

Compared with inorganic crystal modulators, polymeric modulators are expected to have many significant advantages [16], such as high modulation bandwidth, small driving voltage, and low cost. In addition to the high EO coefficients and low dielectric constants, EO polymers offer another unique advantage---their flexibility to fabricate multi-layer thin film structures with ferro-electric domains in any direction of interest. For example, polymer molecules can be aligned in opposite direction within different area of a polymer film during electric poling process [17]. Thus we can get poled areas with alternating domain inversions, i.e. domain-inverted EO polymeric films. In this paper, we report a domain-inverted polymeric Y-coupler modulator with an improved the modulation linearity and larger modulation depth.

Part of the SPIE Conference on Optoelectronic Interconnects VI
San Jose, California • January 1999
SPIE Vol. 3632 • 0277-786X/99/$10.00

The schematic of domain-inverted polymeric modulator is shown in Fig. 1. Basically, this is a modified Y-coupler modulator. Unlike a co-directional coupler, this device has one input and two outputs. The single mode input waveguide branches into a pair of symmetric single-mode waveguides which are optically coupled. The symmetry of the device automatically sets the output of the coupler at the 3dB point without applying driving voltage. In contrast, a conventional modulator, such as Mach-Zehnder interferometer or co-directional coupler, requires either a DC bias or an asymmetric device structure which makes the device construction complicated and causes distortion of linearity due to the DC drift phenomena [13-15]. The new idea of our design is that we used a domain-inverted device configuration. The interaction length L is divided into two equivalent sections. First, the left and right sections of EO polymer film are poled in opposite direction, and then the Y-coupler waveguides are fabricated. The asynchronism introduced in the two sections is equal in magnitude but reversed in sign, i.e., we have $+\Delta\beta$ in the left section and $-\Delta\beta$ in the right when a driving voltage applied to the traveling-wave electrodes deposited on the top cladding layer.

Usually a Y-coupler modulator is characterized by: (1) the interaction length L, (2) the coupling coefficient κ or the coupling conversion length ($lc = \pi/2\kappa$), which is the minimum length required to obtain complete crossover of light power from one branch to another. (3) the mismatch $\Delta\beta = \beta_1 - \beta_2$ of propagation constants β_1 and β_2 between the two waveguides due to the applying of driving voltage. We assume that the energy exchange between the two guides is governed by the coupled-wave equations [18-19]. To simplify, we name the switching state, where the light crosses over completely from one guide to the other, the "cross" state ⊗; and the state in which the light passes straight through, appearing at the output of the same guide, the "bar" state ⊖. We describe the light fields in the two guides by complex amplitudes R(z) and S(z), which vary slowly along the z axis, i.e., the propagation direction. Then

$$\frac{\partial R}{\partial z} - j\delta R = -j\kappa S$$

$$\frac{\partial S}{\partial z} + j\delta S = -j\kappa R$$

Where $\delta = \Delta\beta/2$, and

$$\begin{pmatrix} R \\ S \end{pmatrix} = \frac{1}{\sqrt{2}} \begin{pmatrix} A^* & -jB \\ -jB^* & A \end{pmatrix} \begin{pmatrix} A & -jB \\ -jB^* & A^* \end{pmatrix} \begin{pmatrix} 1 \\ 1 \end{pmatrix} \qquad (1)$$

The matrix coefficients are:

$$A = \cos z\sqrt{\kappa^2 + \delta^2} + j\frac{\delta}{\sqrt{\kappa^2 + \delta^2}} \sin z\sqrt{\kappa^2 + \delta^2}$$

$$B = \frac{\kappa}{\sqrt{\kappa^2 + \delta^2}} \sin z\sqrt{\kappa^2 + \delta^2}$$

So we have the optical power output of the top arm:

$$\left|R^2\right| = \frac{1}{2}\left\{1 - \frac{4xy}{x^2+y^2}\sin^2\frac{\pi\sqrt{x^2+y^2}}{4}\left[1 - \frac{2y^2}{x^2+y^2}\sin^2\frac{\pi\sqrt{x^2+y^2}}{4}\right]\right\} \quad (2)$$

And $|S|^2=1-|R|^2$, the output of the bottom arm.

Where $x= \Delta\beta L/\pi$, the normalized phase shift caused by driving voltage; and $y=L/lc$, the normalized interaction length.

The device is at a cross state, i.e. $|R|^2=0$, when

$$\left(|A|^2 - |B|^2\right) - j\left(2A^*B\right) = 0 \quad (3)$$

Substituting A and B in (3), we get

$$\cos^2\frac{L}{2}\sqrt{\kappa^2+\delta^2} + \frac{\delta^2-\kappa^2-2\kappa\delta}{\kappa^2+\delta^2}\sin^2\frac{L}{2}\sqrt{\kappa^2+\delta^2} - j\frac{\kappa}{\kappa^2+\delta^2}\sin L\sqrt{\kappa^2+\delta^2} = 0$$

Which corresponds to

$$\left(\frac{L}{l}\right)^2 + \left(\frac{\Delta\beta L}{\pi}\right)^2 = 4(2n+1)^2 \quad (4)$$

and

$$\frac{L}{l} = (\pm\sqrt{2}-1)\frac{\Delta\beta L}{\pi} \quad (5)$$

Similarly, the device is at a bar state, i.e. $|R|^2=1$ when

$$\left(|A|^2 - |B|^2\right) - j(2AB) = 0 \quad (6)$$

And we have

$$\cos^2\frac{L}{2}\sqrt{\kappa^2+\delta^2} + \frac{\delta^2-\kappa^2+2\kappa\delta}{\kappa^2+\delta^2}\sin^2\frac{L}{2}\sqrt{\kappa^2+\delta^2} - j\frac{\kappa}{\kappa^2+\delta^2}\sin L\sqrt{\kappa^2+\delta^2} = 0$$

The solution of this condition is

$$\left(\frac{L}{l}\right)^2 + \left(\frac{\Delta\beta L}{\pi}\right)^2 = 4(2n+1)^2 \quad (7)$$

and

$$\frac{L}{l} = (\pm\sqrt{2}+1)\frac{\Delta\beta L}{\pi} \quad (8)$$

These cross states (marked as ⊗) and bar states (marked as ⊖) are represented in the switching diagram of Fig. 2, where we use $x= \Delta\beta L/\pi$ and $y=L/l$ as coordinates for convenience. The cross states are isolated points on the $\pi/8$ and $5\pi/8$ lines through the origin, and the bar states the isolated points on the $3\pi/8$ and $7\pi/8$ lines, correspondingly. While $y=L/l$ value is independent of applied voltage, $x= \Delta\beta L/\pi$ value can be controlled electrically. The driving voltage can drive the points representing the states of the modulator parallel to the x-axis to right or left direction. With the proper values of L/l, the device can be operated as an optical switch. If $y=L/lc=2\sin(\pi/8)$, for example, applied voltage can drive the switch to bar or cross state when $x= \Delta\beta L/\pi=\pm 2\cos(\pi/8)$. Fig. 3 illustrates the optical power output of one branch under different driving

voltage and different interaction length, which were simulated with Equation (2). Clearly we can see that the optical output is set at 3dB point with zero bias. Notice that the modulation depth is different with different interaction length. In Fig. 3 (a), the three curves are corresponding to the optical power outputs when y=1.5, 1.85 (i.e. $2\sin(\pi/8)$), and 2.3. It is interesting that the device fails to response to the modulation when too high driving voltage applied ($\Delta\beta L/\pi >> 1$), where both the outputs of the top and bottom waveguides tend to 50% of the input power again, just as the situation of zero voltage biased.

The linearity of the modulator is significantly improved due to the application of domain-inverted configuration, where the left and right sections are poled in opposite direction. As a result, the high order nonlinear terms cancel each other due to the inverted EO response [20]. Fig. 4 shows the inter-modulation nonlinear distortion (IMD) [20-21] as a function of modulation depth, for both of the domain-inverted Y-coupler modulator and a conventional Y-coupler modulator in which its waveguide is poled only in one direction. When the modulation depth is small, the IMD difference of both structures is little. However, the modulation distortion increases quickly for the conventional modulator while the modulation depth is higher than 30%. In contrast, the IMD of the domain-inverted modulator almost remains at the same level (about -35dB), even when the modulation depth is as high as 99%.

We used BPM software to determine the waveguide dimensions, coupling inversion length, and the angle between the Y-branches. In our experiment, the refractive indices of EO polymer and cladding materials are 1.5565 and 1.5420, respectively, at the operation wavelength of 1.3μm. The thickness of the channel waveguide was controlled around 2.6 μm for single mode operation. Simulation shows the cutoff width for a single mode waveguide is 5.7 μm. We used 4 μm as the channel width to get a larger channel spacing aimed at improving the fabrication tolerance of the microwave electrodes. Fig. 5 shows the simulated results to determine the coupling inversion length of the coupler. When the channel spacing is 6 μm, the coupling inversion length lc was 10.2 mm. In our devices, we used an interaction length of $L = 2lc \sin(\pi/8) = 19.2$ mm to reach the optical switching status (Ref. Fig. 2).

Optimizing the Y-coupler angle between the two branches is another critical factor in the device design. Too large angle will cause more radiation loss near the splitting bends of the waveguides and reduce the coupling efficiency. Fig. 6 illustrates the simulated results with BPM. According to Fig 6(c), the better choice for the angle is between 0.5 and 1 degree. In our design, we used an angle of 0.6°, corresponding to an S-bend length of 1mm.

The EO polymer used for our device was a polyimide-based chlorophenol red, with a 20% weight loading of chromophore. The glass transition temperature of this host-guest system is 235 °C. Its absorption spectra shows a peak around 430 nm We used Ultradel 9120D (Amoco Chemical) as top and bottom cladding layers. The refractive indices of EO polymer and cladding are 1.5565 and 1.5420 (λ =1.3 μm), respectively, after the poling process. Excellent EO polymer films, with a thickness of 2~3μm, were obtained by spin-coating the polymer on the Ultradel 9120 cladding layer. Fig. 7 is a photo that a laser beam of 1.3μm wavelength was coupled into the planar EO polymer waveguide with a small prism. A propagation loss of 0.43dB/cm was measured.

The corona poling, a typical technique to align the EO polymer molecules [22], is not suitable to make domain-inverted devices. In corona poling, a high electric field is produced by the charge dropped on the film surface through the corona discharge process. Therefore, the electric field can only point in one direction, not two opposite directions as desired for domain inversion. Besides, it is very difficult to precisely control the poling area under the electric corona. Therefore we used a domain-inverted poling technique based on the combination of liquid-contact poling and pulse poling technique developed in our group [17,23], as illustrated in Fig. 8. First, the three polymer layers were spin-coated on Si wafer with a thin layer of Au as the ground electrode for poling. The bottom and top cladding layers (Ultradel 9120D, an excellent photo-polyimide) were cured with UV light. After drying the sample in vacuum oven at 150° for 5 hours, cover the sample with two pieces of ITO slides. There was a narrow insulator spacer of 0.5 mm between the two ITO slides. In order to prevent poling sparks, a thin layer of conductive liquid was applied between the ITO slides and the top cladding layer. The ITO slides and the thin Au film on Si wafer served as poling electrodes. The sample was set on a hotplate, heated to 230 °C first. Then the pulse poling electric fields, with opposite direction, were applied to the sample. We used a computer controlled power supply, applied the positive and negative pulse voltages to the left and right sections alternately, i.e. when left side was on (off), right side off (on), with equal time period and voltage amplitude. After 40 minutes, turned off the power of the hotplate, and let the sample cooled down to room temperature while keeping the poling voltage on. The peak-to-peak pulse voltage was 1500V with a period of 0.1 second. The total thickness of polymer layers was 8~9 μm, so the average poling strength was about 160 V/ μm.

Fig. 9 illustrates the device fabrication procedures. The rib Y-coupler channels were made using the normal photolithography and oxygen reactive ion etching (RIE) techniques with the sample poled as above. After adding a thin layer of top cladding, the Au driving electrodes were deposited and patterned. Fig. 10 shows parts of the RIE etched channels and electrodes. The channel end-faces were prepared by dicing and polishing before testing. The device was 2.5 cm in long with a 19.2 mm of interaction length for the electrodes.

Fig. 11 is a photo of the testing setup. The sample was set on a 4-axis stage for fine adjustment. A laser beam of 1.3μm wavelength was launched into and the device through a 40x microscope objective. The output light was coupled out through another 40x objective and received by a photo-detector. A CCD camera was employed at the same time to measure the distribution of optical output field. Fig. 12 shows the measured optical power out of one branch of the modulator versus the driving voltage. The half power point was automatically set without applying voltage. The modulator was driven into extinction at 12V with a switching depth of 23 dB. Fig. 13 shows the 3-D near-field output patterns when the driving voltage were zero and 12V. The EO coefficient was determined to be about 9.5 pm/V for this EO polymer system.

In conclusion, we have demonstrated a polymeric Y-coupler modulator with a domain-inverted configuration. The modulation linearity was improved due to the novel device structure. The Y-coupler modulator was automatically set at 3dB point without applying any DC bias. At the same time, a domain-inversion poling technique was developed, which can be used to fabricate other novel type of active EO devices in the future.

This work was supported by AFOSR and BMDO.

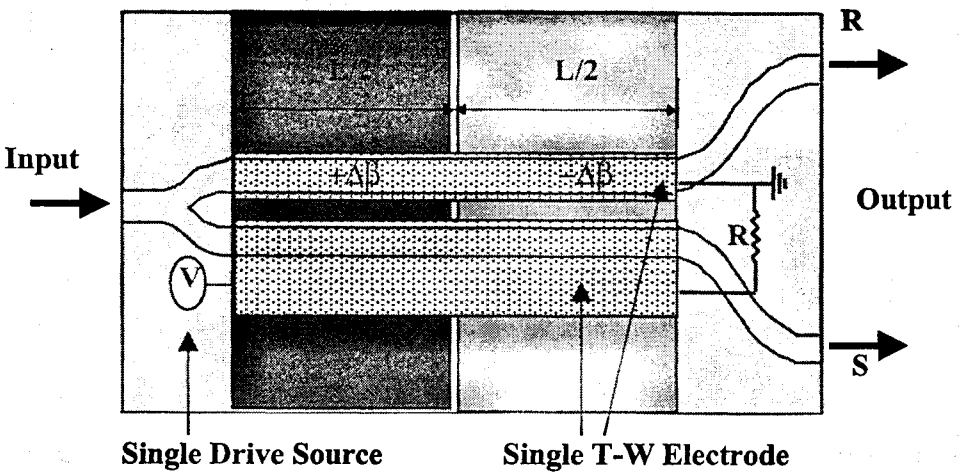

FIG. 1 Schematic of domain-inverted Y-coupler modulator.
The left and right sections are poled in opposite direction

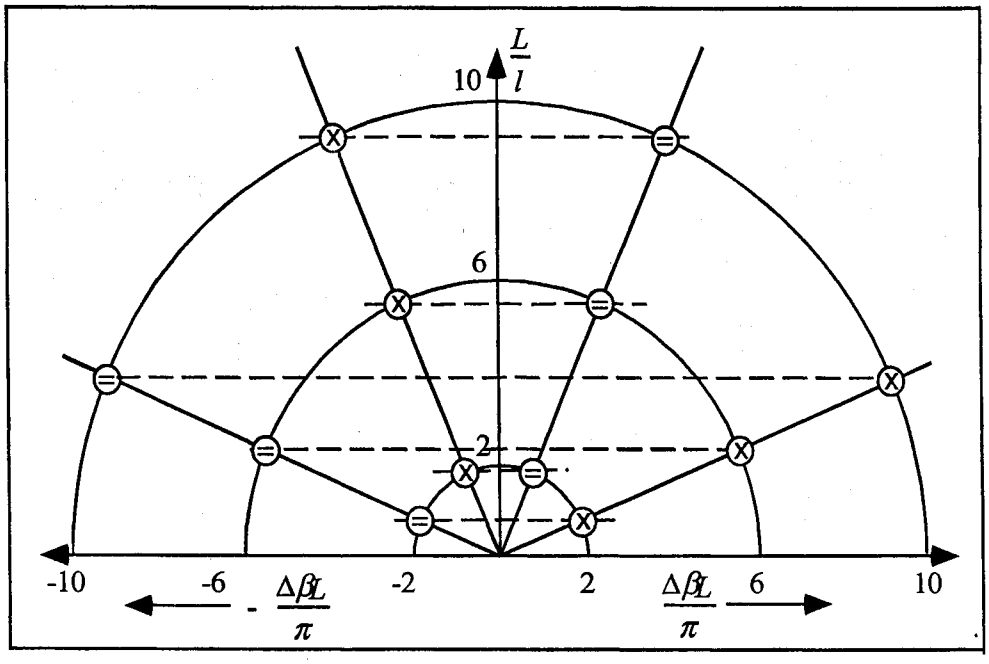

FIG. 2 Switching diagram of the domain-inverted modulator. The bar ⊖ and cross ⊗ states are represented with the isolated points on the lines through origin, respectively.

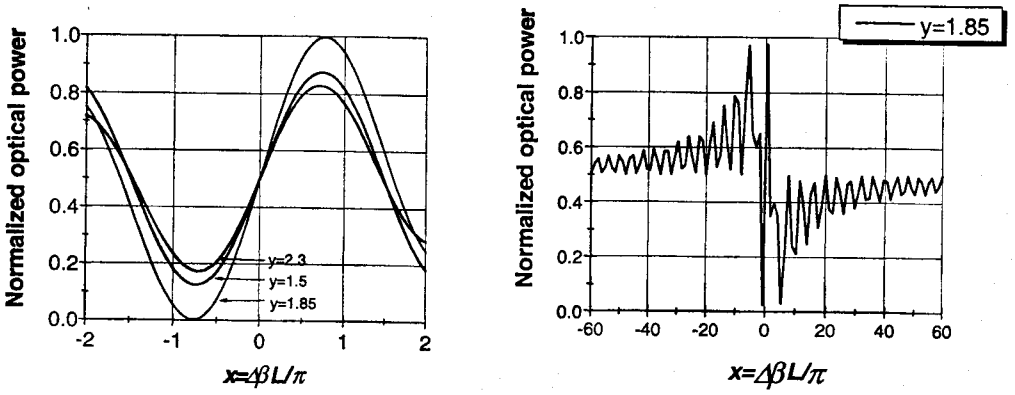

FIG. 3 Simulated optical power output as a function of the normalized phase mismatching when the driving voltage is (a) $\Delta\beta L/\pi \leq 2$, low voltage and (b) $\Delta\beta L/\pi \leq 60$, high voltage. Modulator is set at 3 dB point with zero bias.

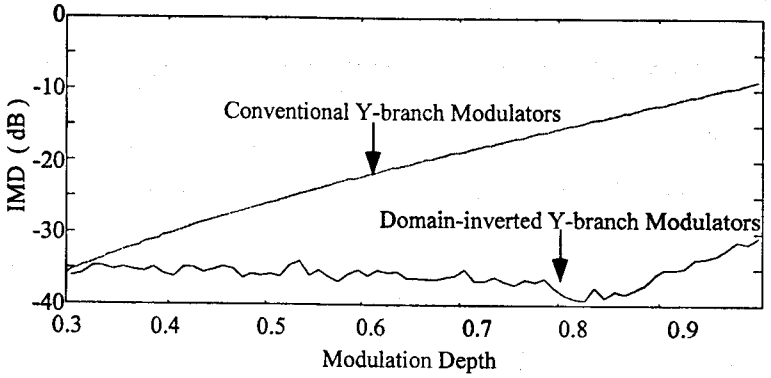

FIG. 4 Inter-modulation distortions for domain-inverted Y-coupler modulator and conventional modulator versus the modulation depth. Data for Simulation : EO polymer n_1=1.5565, r_{33} =24 pm/V; cladding polymer n_2=1.542; Channel section: 4μm x 2.6 μm, Channel spacing: 6 μm; λ=1.3 μm.

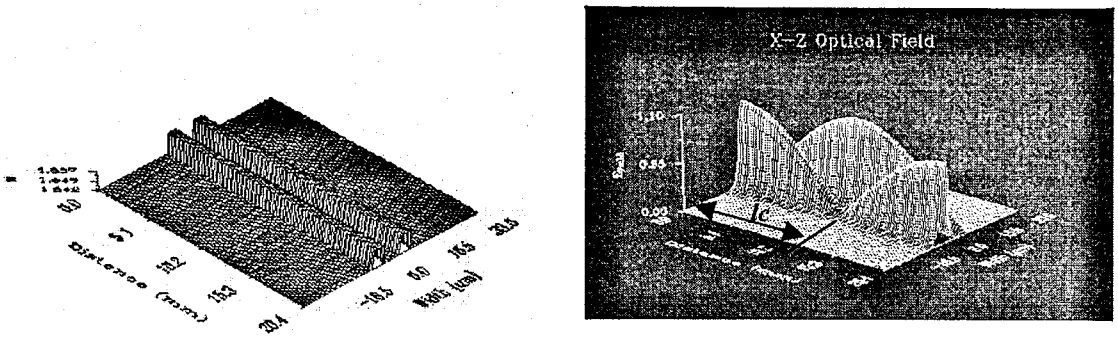

(a) co-directional waveguides (b) Simulated result for coupling length *lc*

FIG. 5 The coupling inversion length of the directional waveguides. With the same data used in Fig 4, a coupling length of *lc*=10.2 mm was obtained.

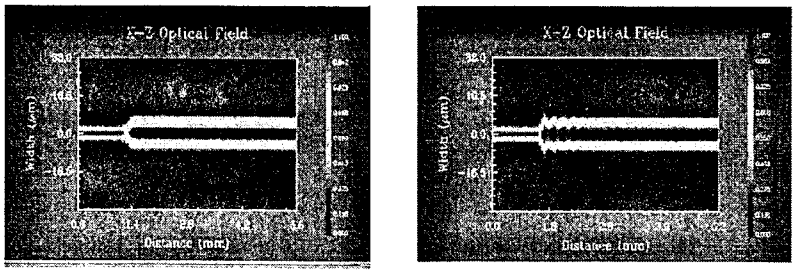

(a) α=1° (b) α=3°

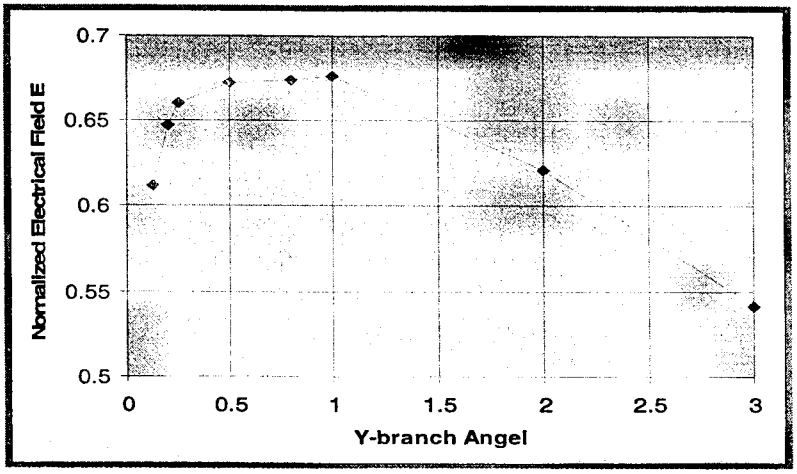

(c)

FIG. 6 Radiation loss versus the Y-branch angle. Notice the larger loss at the branch shoulder in (b). The better angle is between 0.5° to 1°

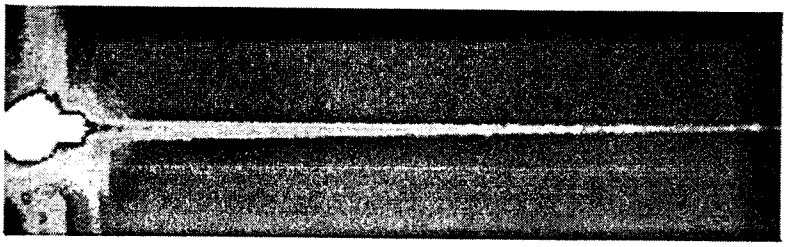

FIG. 7 Photo of EO polymer planar waveguide, coupled with mini-prism. 0.34 dB/cm propagation loss was measured at wavelength of 1.3 μm.

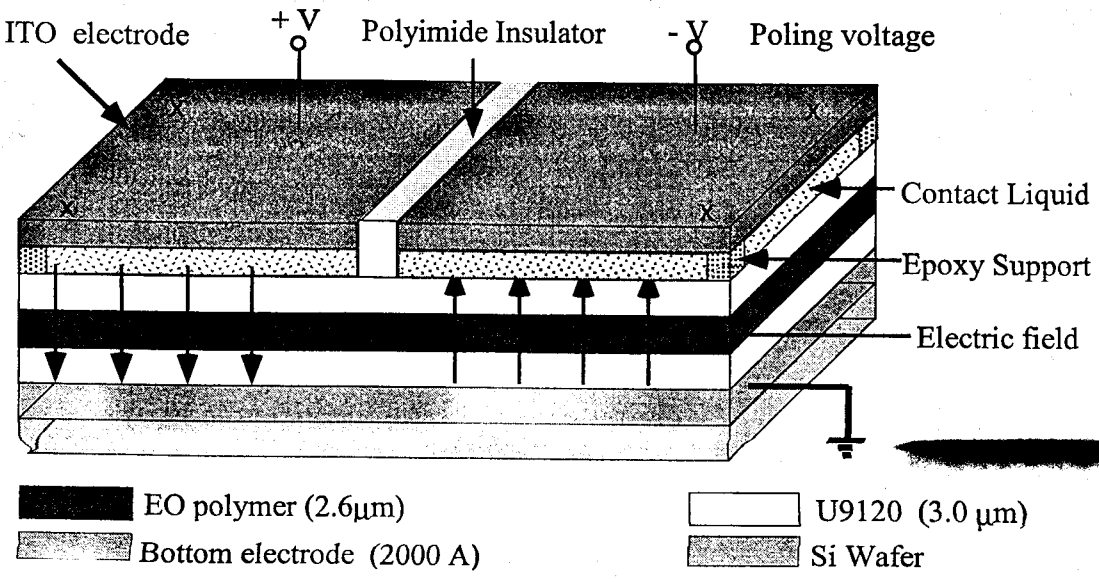

FIG. 8 Schematic of domain-inverted poling using liquid-contact technique

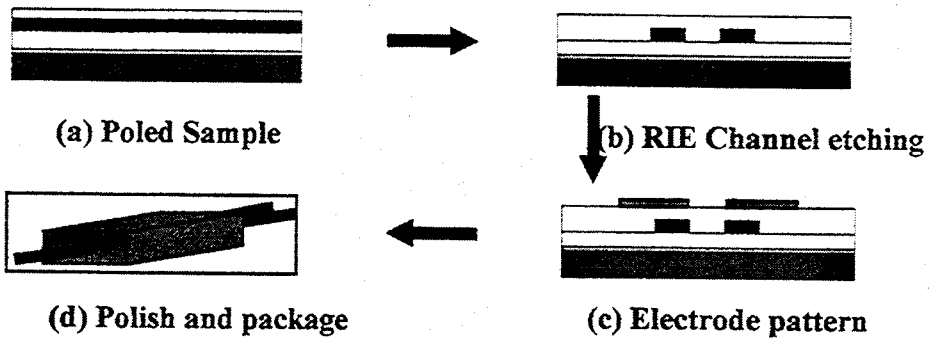

FIG. 9 Device fabrication processes

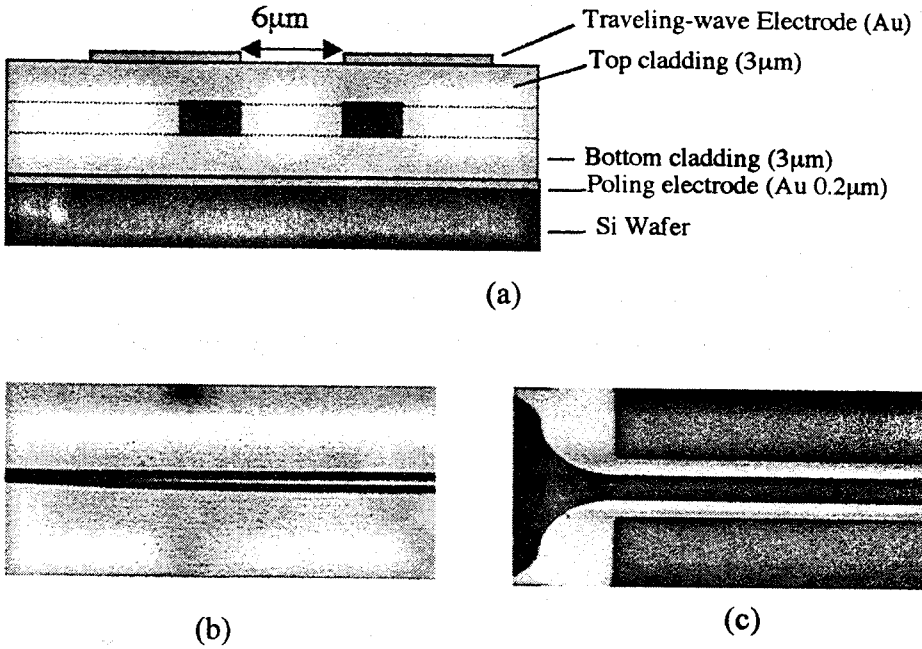

FIG. 10 Device structures. (a) Channel end-section view. Channel size: 4 x 2.6 μm
(b) photo of RIE etched channel, near the splitting area. (c) photo of modulating electrodes on top of the cladding layer covering over the Y-branch waveguides

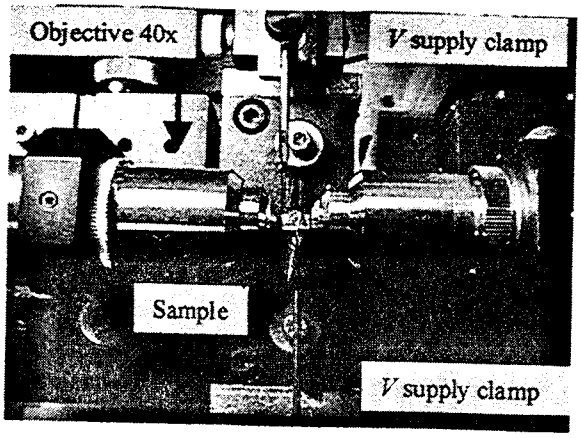

FIG. 11 Modulator testing setup

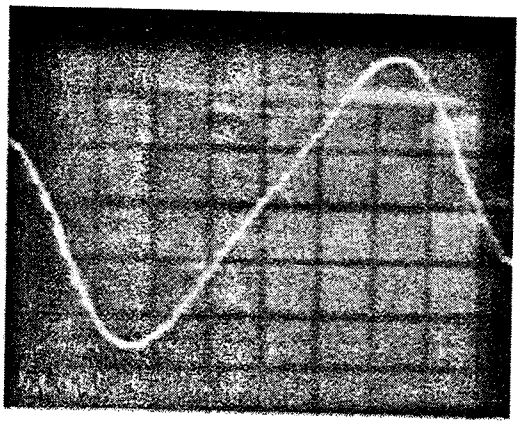

FIG. 12 Modulator optical power output of one branch versus the driving voltage. Switching voltage of 12v observed.

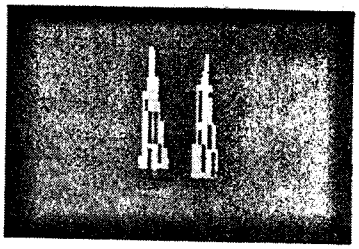

(a) V =0

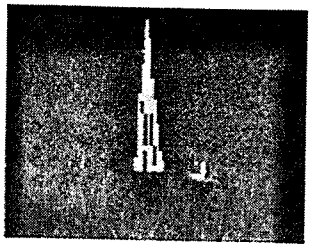

(b) V =12 (V)

FIG. 13 3-D output patters out of the two branches of the modulator with (a) zero bias and (b) 12v bias, where one branch was switch off.

REFERENCES

1. Rod. C. Alferness, Integrated Photonics Research, 7, paper L2-1, Dana Point, CA, 1995.
2. R. C. Alferness, IEEE Trans. Microwave Theory Tech., **MTT-30** (8), pp. 1121, 1982.
3. H. Nagata and J. Nayyer, OSA/IEEE Integrated Photon. Research, Technical Digest Series, **7**, 290, 1995.
4. J. H. Schaffner, W. B. Bridges, Proc. SPIE, **2155**, pp. 218-228, 1995.
5. Kazuto Noguchi, Osamu Mitomi, Hiroshi Miyazawa, and Shunji Seki, J. of Lightwave Technol., **13**, pp. 1164-1166, 1995.
6. C. H. Bulmer and W. K. Burns, J. Lightwave Technol., **LT-1**, pp.227-236, 1993.
7. Juan F. Lam and Gregory L. Tanggonan, IEEE Photon. Technol. Lett., **3**, pp. 1102-1104, 1991.
8. Antao Chen, Vadim Chuyanov, Sean Garner, Hua Zhang, W. R. Steier, J. Chen, J, Zhu, F. Wang, M. He, S. Mao, and L.R. Dalton, Optics Letters, **23** (6) pp. 478-80, 1998.
9. Yongqiang Shi, W. Wang, J. H. Bechtel, A. Chen, S. Garner, S. Kalluri, W.H. Steier, D. Chen, and H.R. Fetterman, IEEE J. Sel. Top. Quantum electron. **2**, pp. 289, 1996.
10. Paul R. Ashley, Proc. SPIE, **2290**, pp. 114-124, 1994.
11. D.G. Girton, S.L. Kwiatkoski, S.F. Lipscomb, R.S. Lytel, Appl. Phys. Lett., **58**, pp. 1730 , 1991.
12. T. A. Tumolillo, Pau R. Ashley, Appl. Phys. Lett, **62** (24), pp. 3068-1070, 1993.
13. Y. Shi, W. Wang, W. Lin, D.J. Olson, and J.H. Bechtel, Appl. Phys. Lett, **71**(16), pp. 2236, 1997.
14. Heuk Park, Wol-yon Hwang, and J.J. Kim, Proc. SPIE, **2852**, pp. 286, 1996.
15. R.A. Becker, Optics Letters, **10**, pp. 417, 1985.
16. H.S. Nalwa and S. Miyata, "*Nonlinear Optics of Organic molecules and polymers*", CRC Press, Boca Raton, 1996.
17. Jeffery J. Maki, Guohua Cao, John M. Taboada, Huajun Tang, Suning Tang, and Ray T. Chen, Proc. SPIE, **3281**, pp. 55, 1998.
18. Herwig Kogelnik and Ronald V. Schmidt, IEEE J. of Quantum Electron., QE-**12**, pp. 396-401, 1986.
19. S. Thaniyavarn, Electron. Lett., **22**, pp. 941-942, 1986.
20. Gray E. Betts, L. M. Walpita, W . S. C. Walpita, W. S. C. Chang, and R. F. Mathis, J. of Quantum Electron., QE-**22**, pp. 1009-1011, 1996.
21. B. H. Kolner and D. W. Dolfi, Appl. Opt., **26**, pp. 3676-3680, 1989.
22. R. A. Hill, A. Knoesen, and M. A. Mortazavi, Appl. Phys. Lett., **65** (14), pp. 1733, 1994.
23. Zuozhou Yue, Dechang An, and Ray T. Chen, Appl. Phys. Lett., **72**(26), 3420, 1998.

Invited Paper

Si CMOS Process-compatible Guided-wave Optical Interconnects

R. T. Chen[1], L. Wu[1], L. Lin[1], C. Choi[1], Y. Liu[1], B. Bihari[1], S. Tang[2], R. Wickman[3], B. Pecor[3] and Y. S. Liu[4]

[1]Microelectronics Research Center
JJP Research Campus
University of Texas, Austin
Austin, TX 78758
Raychen@uts.cc.utexas.edu

[2]Radiant Research
Braker Lane Suite 420
Austin, TX 78759

[3]Cray Research
1050 Lowater Road
Chippewa, WI 54729

[4]GE Research and Development Center
1 River Rd. Schenectady, NY 12345

Abstract

We report the formation of polyimide-based H-tree waveguides for a multi-GBit/sec optical clock signal distribution in a Si CMOS process compatible environment. Such a clock distribution system is to replace the existing electronic counterpart associated with high-speed supercomputers such as Cray T-90 machine. A waveguide propagation loss of 0.21 dB/cm at 850 nm was experimentally confirmed for the 1-to-48 waveguide fanout device. The planarization requirement of the optical interconnection layer among many electrical interconnection layers makes the employment of tilted grating a choice of desire. Theoretical calculation predicts the 1-to-1 free-space to waveguide coupling with an efficiency as high as 95%. Currently, a coupling efficiency of 35% was experimentally confirmed due to the limited index difference between guiding and cladding layers. Further experiments aimed at structuring a larger guiding/cladding layer index differences are under investigation. To effectively couple an optical signal into the waveguide through the titled grating coupler, the accuracy of the wavelength employed is pivotal. This makes the usage of the vertical cavity surface-emitting lasers (VCSELs) and VCSEL arrays the best choice when compared with edge-emitting lasers. Modulation bandwidth as high as 6 GHz was demonstrated at 850 nm. Such a wavelength is compatible with Si-based photodetectors.

The speed and complexity of integrated circuits are increased rapidly as integrated circuit technology advances from very large scale integrated (VLSI) circuits to ultra large scale integrated (ULSI) circuits. As the number of components per chip, the number of chips per board, the modulation speed and the degree of integration continue to increase, electrical interconnects are facing their fundamental bottle-necks, such as speed, packaging, fanout, and power dissipation. Multichip module (MCM) technology is employed to provide higher clock speeds and circuit densities[1,2]. However, the state-of-the-art technologies based on electrical interconnects fail to provide the required multi-GBit/sec clock speed and communication distance in intra-MCM and inter-MCM hierarchies.

For a multiprocessor computer system, such as a Cray T-90 supercomputer, it is extremely difficult to obtain high-speed (>500 MHz) synchronous clock distribution using electrical interconnections due to large fanouts (48x2) and long interconnection lengths (>15 cm)[3-7]. A fanout chip is required to provide the massive electrical fanout. The synchronous global clock signal distribution is highly desirable to simplify the architecture and enable a higher speed performance. High-speed, large-area massive fanout optoelectronic interconnects may overcome many of the problems associated with electrical interconnects in this interconnection scenario[3-11]. An array of novel optical interconnect architecture has been proposed and then demonstrated by earlier researchers[11-14], which may partially satisfy the above requirements for a massive clock signal distribution in intra-MCM and inter-MCM hierarchies.

Part of the SPIE Conference on Optoelectronic Interconnects VI
San Jose, California • January 1999
SPIE Vol. 3632 • 0277-786X/99/$10.00

In this paper, we report the development of a planarized guided-wave optoelectronic interconnect network for optical clock signal distribution on a board-level multi-processor system. The electrical interconnect network currently employed by Cray Research is shown in Fig. 1 which shows the existing 500 MHz 1-to-48 clock signal distribution (one side) realized in one of the 52 vertical integration layers (not shown) within the Cray-T-90 supercomputer board.

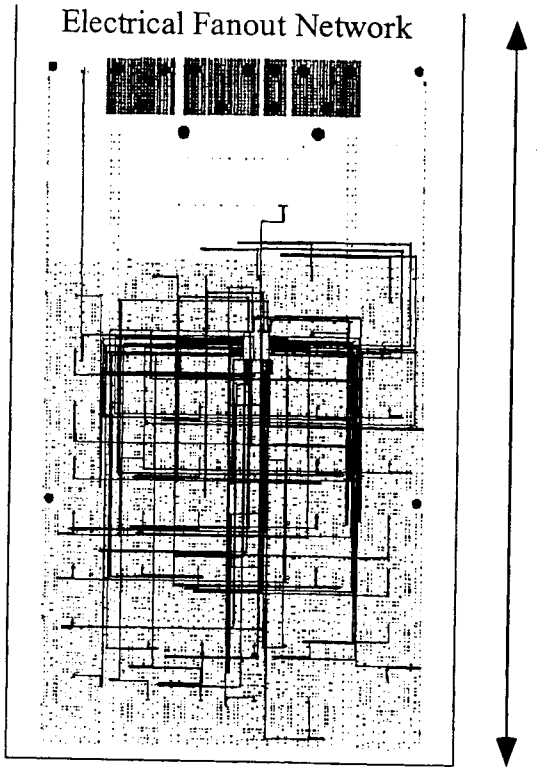

Fig. 1 Schematic diagrams of massive clock signal distribution networks using an electrical clock signal transmission line network that forms one of the 52 layers of Cray T-90 Supercomputer board. The holes indicate the feed-through marks of the on-board 3-D interconnect.supercomputer system may have a clock speed more than ten times higher than current systems.

To further upgrade the clock speed, an appropriate optical interconnect scheme has to be incorporated. In this paper, an integrated board-level optoelectronic interconnection layer is constructed by using polyimide-based optical channel waveguides in conjunction with tilted waveguide gratings. This guided-wave optoelectronic interconnect network is to be inserted into the Cray supercomputer boards to become an additional optical interconnection layer among many other electrical interconnection layers.

Our approach is to construct an additional optoelectronic interconnection layer (OIL) for the high-speed optical clock signal distribution using polymer-based guided-wave devices. The selection of guided-wave approach is mainly based on the system alignment and reliability concerns[15]. During the course of research, Si CMOS process compatibility and planarization of the OIL are the two major technical concerns. A polymer-based waveguide H-tree system is employed to replace the existing electrical fanout interconnect network shown in Fig. 2. The optical clock signal delivered by an optic fiber will be coupled into the OIL using an input surface-normal tilted grating coupler, and distributed through out the board by the polymer-based channel waveguide network. The distributed optical clock signal at each fanout end will be coupled into a Si photodetector by an output surface-normal grating coupler.

The building blocks required to necessitate such an optical H-tree system include high performance low-loss polymer-based channel waveguides, waveguide gratings, 1-to-2 3 dB waveguide splitters and curved waveguides. These components allow the formation of a waveguide H-tree for the required optical clock signal distribution, where all the optical paths have the same length to minimize the clock skew problem. The employment of optical channel waveguides and surface-normal waveguide gratings provides a compact, mechanically reliable system. Due to the nature of massive fanouts (48x2) over a large area, the waveguide propagation loss must be minimized while the waveguide grating coupling efficiency has to be maximized. These two factors are very important to ensure enough optical power at the end of photodetectors for high-speed operation. We have employed the highly purified version of the commercially available polyimides in order to fabricate low-loss polymeric waveguides. To improve the waveguide grating coupling efficiency, tilted waveguide gratings are employed to provide the required 1-to-1 surface-normal coupling. Note that a simple 45° waveguide end mirror is not suitable in this case because of the requirement of planarization imposed on the vertical integration of the other electrical interconnection layers[16,17].

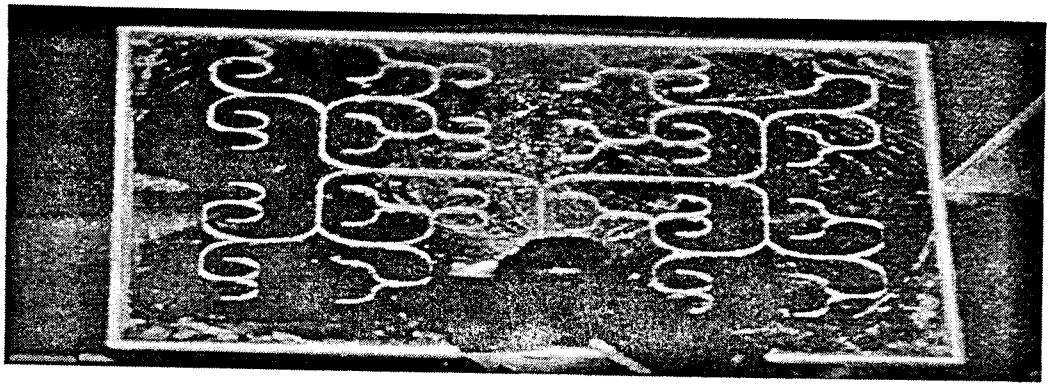

Fig.2 Photograph of the 1-to-48 fanout H-tree Polyimide-based waveguide on quartz

While fiber optics technology has successfully implemented among cabinets as replacements for coaxial cable point-to-point link, its application inside a cabinet on the MCM system is severely limited due to the bulkiness of fibers, fiber connectors, and significant labor and cost involved in parallelism of the interconnects. Polymer optical waveguide technology, on the other hand, is particularly suitable for wafer-scale MCM interconnect applications for its large area waveguide formation and potential low costs. It can be viewed as an optical equivalent of electrical printed wiring board technology in which the fabrication cost is independent of the interconnect functionality and complexity. In order to take the advantages of the polymer waveguides, we must be capable of implementing optoelectronic devices such as laser diodes, and photodetectors in the same MCM package. If optical waveguides can be fabricated, integrated, and packaged into the MCM with existing electronic MCM fabrication technologies, the insertion of optical interconnects becomes an acceptable approach to upgrade the microelectronics-based high performance computers.

Both the waveguides and the tilted gratings are polyimide-based to provide the high temperature processing requirement associated with Si CMOS fabrication. The modulation source that converts electrical signals to optical signals is realized using vertical cavity surface emitting lasers (VCSELs) and VCSEL arrays with a modulation bandwidth of 6 GBit/sec. The power budget consideration is also investigated with appropriate light source allocations to meet the bit error rate (BER) requirement.

In order to fabricate the grating coupler by reactive-ion-etching (RIE), a thin aluminum metal mask was deposited on top of the polyimide-based planar guide. The schematic diagram for the fabrication process is shown in Fig.3. First, a 500-Angstrom aluminum layer was coated on top of the waveguide by electron beam evaporation, followed by a layer of 5206E photoresist with a spin speed of

3000 rpm. The grating patterns on photoresist were recorded by interfering two beams at λ=442 nm (a He-Cd laser line). To record a grating with a period of Λ, the cross angle θ of the two interference beams is determined through the formula of $\sin(\theta/2) = (\lambda/\Lambda)$. After the sample had been developed, a postbake at 120^0C for 30 minutes was followed. To transfer the photoresist grating patterns to aluminum, we used RIE to remove the aluminum in the window region of the photoresist pattern. The gases used were $BCl_3/SiCl_4$ with a pressure of 20 millitorr. To form the tilted grating pattern on the polyimide waveguide, we used a RIE process with a low oxygen pressure of 10 millitorr to transfer the grating pattern on aluminum layer to the polyimide layer. In order to get the tilted profile, a Faraday cage was used. The final step was to remove the aluminum mask by another step of RIE process. Microstructures of the tilted grating having a periodicity varying from 0.5 μm to 3 μm have been fabricated. Fig. 4 shows one of many gratings from a scanning electron microscope (SEM) picture.

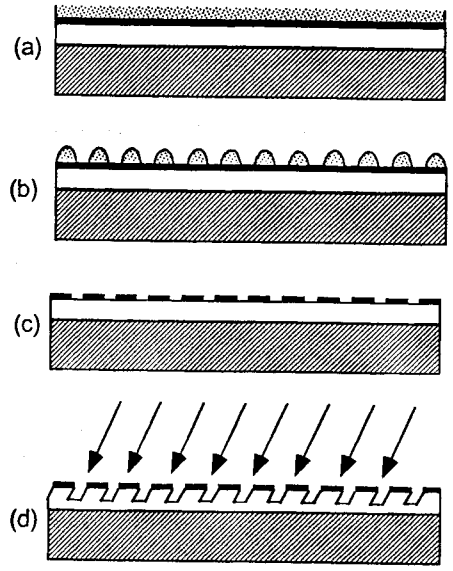

Fig. 3 The schematic diagram for the fabrication of tilted grating on polyimide waveguide.

A test waveguide sample with a tilted grating as the surface-normal input coupler was built using 632.8 nm as the operating wavelength [18]. The schematic of coupling a surface-normal input light into a waveguide using the device fabricated is shown in Fig. 4(a), together with an experimental photograph in Fig. 4(b). The grating is designed to surface-normally couple the laser beam into the waveguide with an operating wavelength at 632.8 nm. The coupling to the planar waveguide with the unidirectional propagation can be clearly observed with a measured efficiency of 35%. This is our first device employing the surface-normal waveguide input coupling. Note that the index difference between the guiding layer and the substrate layer is less than 0.03 for the device shown in Figure 4. Theoretical result shows that the index difference between the guiding and the cladding layers plays an important role in enhancing the coupling efficiency. Further research aimed at providing a larger index difference to increase the coupling efficiency is under investigation.

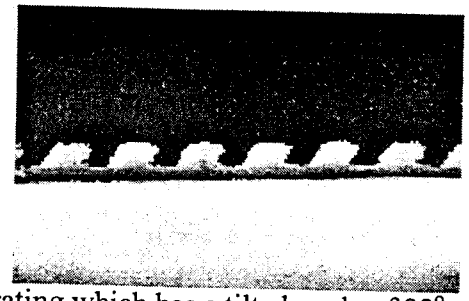

Fig. 4 SEM picture of a tilted grating which has a tilted angle of 32°. Grating periods from 0.5 μm to 3 μm have been successfully fabricated with an aspect ratio of 1.1.

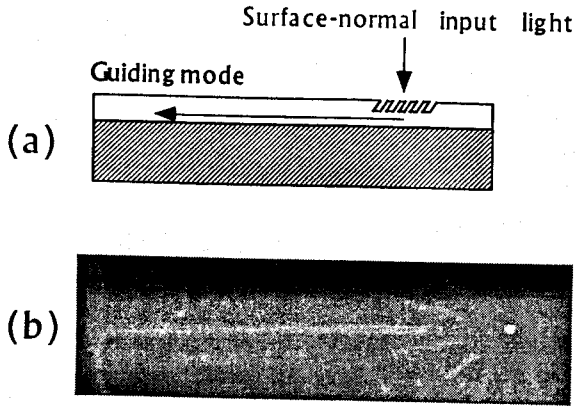

Fig. 4 (a) The schematic of coupling a surface-normal input light into waveguide using the tilted grating. (b) The experimental photograph of coupling a surface-normal input 632.8 nm He-Ne light into the polyimide waveguide.

Because the Cray supercomputer board is 26.67 cm in length, which is beyond the field size of the in-house microlithography, large-area optical waveguides are required to build an optical clock signal distribution layer. To meet the size requirement, a laser beam direct writing was employed to solve the problem. The laser-beam writing system consists of a dual-wavelength HeCd laser (λ_1 = 325 nm and λ_2 = 442 nm), beam-shaping optics, an electronic shuttle and a computer-controlled X-Y-Z translation stage

This research is sponsored by ONR, BMDO, DARPA's center for optoelectronics science and technology, the ATP program of the state of Texas, 3M Foundation, Cray Research, GE, Honeywell and MCC.

References

1. D. P. Seraphim and D. E. Barr, "Interconnect and packaging technology in the 90's," Proc. SPIE 1390, pp. 39-54, 1990.
2. C. Neugerbauer, R. O. Carlson, R. A. Fillion, and T. R. Haller, "Multichip module designs for high performance applications," in Multichip Modules, Compendium of 1989 Papers, pp. 149-163, International Electronic Packaging Society, 1989.
3. J. W. Goodman, F. I. Leonberger, S. Y. Kung, and R. A. Athale, "Optical interconnections for VLSI systems," Proc. IEEE 72, pp. 850-866, 1984.
4. M. R. Feldman, S. C. Esener, C.C. Guest, and S. H. Lee, "Comparison between optical and electrical interconnects based on power and speed considerations," Appl. Opt., vol. 27, pp. 1742-1751, 1988.

5. Founad E. Kiamilev, Philippe Marchand, Ashok V. Krishnamoorthy, Sadik C. Esener, and Sing H. Lee, "Performance comparison between optoelectronic and VLSI multistage interconnects networks," IEEE J. of Light. Technol., vol. 9, pp. 1674-1692, 1993.
6. Paola Cinato, Kenneth C. Young, Jr., "Optical interconnections within multichip modules," Opt. Eng., vol. 32, pp. 852-860, 1993.
7. Bradley D. Clymer and Joseph W. Goodman, "Optical clock distribution to silicon chips," Opt. Eng., vol. 25, pp. 1103-1108, 1986.
8. Suning Tang, Ray T. Chen and Mark Peskin, "Packing density and interconnection length of a highly parallel optical interconnect using polymer-based single-mode bus arrays," Opt. Eng., vol. 33, pp. 1581-1586, 1994.
9. Ray. T. Chen, Suning Tang, T. Jannson and J. Jannson, "A 45 cm long compression molded polymer-based optical bus," Appl. Phys. Lett., vol. 63, pp. 1032-1034, 1993.
10. Ray T. Chen, "Polymer-based Photonic Integrated Circuits," (Invited Review Paper), *Optics and Laser Technology*, Vol. 25, pp. 347-365(1993).
11. Ray. T. Chen, H. Lu, D. Robinson, Michael Wang, Gajendra Savant, and Tomasz Jannson, "Guided-wave planar optical interconnects using highly multiplexed polymer waveguide holograms," IEEE J. Light. Technol., vol. 10, pp. 888-897, 1992.
12. R. W. Wickman, "Implementation of optical interconnects in GibaRing supercomputer channel", Proc. SPIE, vol. CR62, pp. 343-356, 1996.
13. M. R. Feldman, "Holographic optical interconnects for multichip modules," Proc. SPIE, vol., 1390, pp. 427-433, 1990.
14. Suning Tang and Ray T. Chen, "1-to-42 optoelectronic interconnection for intra-multichip-module clock signal distribution," Appl. Phys. Lett., vol. 64, pp. 2931-2933, 1994.
15. Sunny Bains, "Optical interconnects are taking off as the data transport of tomorrow," OEM Magazine, pp. 48-53, July 1996.
16. Y. S. Liu, W. Hennessy, R. Wojnarowski, J. Bristow, Y. Liu, J. Rowlette, J. Stack, J. Yardley, L. Eldada, R. M. Osgood, R. Scarmozzino, S. H. Lee and S. Patra, "Optoelectronic Backplane Interconnect Technology Development," Proc. SPIE, Optoelectronic Interconnects and Packaging IV, Editor: Ray Chen and P. Guilfoyle, pp.2-10, Vol.3005, 1997.
17. K. S. Giboney, "Parallel-optical Interconnect Development at HP Laboratories," Proc. SPIE, Optoelectronic Interconnects and Packaging IV, Editor: Ray Chen and P. Guilfoyle, pp.193-201, Vol.3005, 1997.
18. Toshiaki Suhara and Hiroshi Nishihara, "Integrated optics components and devices using periodic structures," IEEE J. of Quantum Electronics, vol. QE-22, no. 6, pp. 845-867, 1996.